03567

AERODYNAMIC DRAG ON SPIKED BLUNT BODIES IN LOW-DENSITY HYPERSONIC FLOW

By

William H. Sims and Jerry S. Hahn

von Kármán Gas Dynamics Facility

ARO, Inc.

TECHNICAL DOCUMENTARY REPORT NO. AEDC-TDR-64-160

August 1964

Program Element 62405334/8953, Task 895306
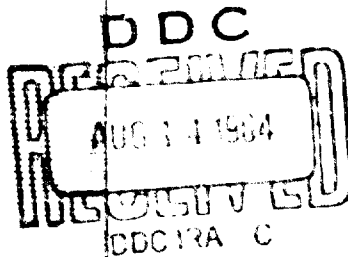
D D C

AUG 1 4 1964

CDC TRA C

ARNOLD ENGINEERING DEVELOPMENT CENTER

AIR FORCE SYSTEMS COMMAND

UNITED STATES AIR FORCE

NOTICES

AERODYNAMIC DRAG ON SPIKED BLUNT BODIES IN LOW-DENSITY HYPERSONIC FLOW

By

William H. Sims and Jerry S. Hahn

von Kármán Gas Dynamics Facility

ARO, Inc.

a subsidiary of Sverdrup and Parcel, Inc.

August 1964

ARO Project No. VL2407

ABSTRACT

Aerodynamic drag on spiked blunt bodies has been measured in hypersonic, low-density flow of nitrogen. Two models were tested: a spherically capped cone of 10-deg half-angle at $0 \leq \alpha \leq 40$ deg, and a right circular cylinder at $\alpha = 0$. Reynolds numbers, based on total body lengths and free-stream conditions, varied from 200 to 1200. Mach number was constant at 10.1.

Results have been compared with modified Newtonian and free-molecule calculations. Effects of hypersonic rarefied flow are apparent, with drag coefficient increasing for large angles of attack for all spike lengths. A correlation procedure suggested in an earlier report for a large class of similar bodies at 0-deg angle of attack is shown to be effective in the case of spiked bodies too. It is apparent that the marked reduction of drag effected by use of spikes on blunt-nosed bodies at higher Reynolds numbers is greatly diminished when low Reynolds numbers exist. However, a moderate reduction is shown for small angles of attack at the Reynolds numbers of the present experiment.

PUBLICATION REVIEW

This report has been reviewed and publication is approved.
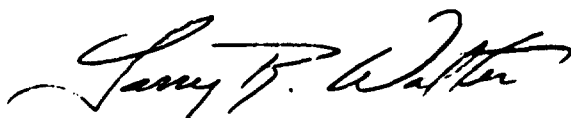
Larry R. Walter
1st Lt, USAF
DCS/Research

Donald R. Eastman, Jr
DCS/Research

CONTENTS

ILLUSTRATIONS

NOMENCLATURE

C_∞	Chapman-Rubesin Constant, $(\mu_w T_\infty)/(\mu_\infty T_w)$
C_D	Drag coefficient, $D/(q_\infty S)$
$C_D{}^*$	Normalized drag coefficient, $(C_D - C_{D_i})/(C_{D_{FM}} - C_{D_i})$
C_{D_i}	Inviscid-fluid drag coefficient
D	Aerodynamic drag force, or diameter
L	Model characteristic length; length measured along surface from forward stagnation point to base
M	Mach number
$\dot{m}$	Mass flow
p	Pressure
Re_∞, D	Reynolds number based on body diameter and free-stream conditions
Re_∞, L	Reynolds number based on length L and free-stream conditions
T	Temperature
U	Velocity
$\overline{V}_\infty$	Viscous interaction drag parameter, $M_\infty \sqrt{C_\infty/Re_\infty, L}$
x	Axial coordinate relative to nozzle exit, zero at exit, positive downstream
y	Radial coordinate relative to nozzle centerline, zero on centerline, positive upward
α	Angle of attack
γ	Ratio of specific heats
μ	Viscosity
ρ	Density

SUBSCRIPTS

o	Isentropic stagnation conditions. When used in combination with a prime $(p_o{}')$, conditions at the stagnation point on a body are referred to.
FM	Free-molecule condition

i	Inviscid value
L	Based on model characteristic length
w	Wall conditions
∞	Free-stream or test section conditions

1.0 INTRODUCTION

The aerodynamic characteristics of blunt bodies fitted with spikes or "windshields" have been studied extensively with the purpose of reducing the drag forces and heating rates on the bodies (Refs. 1-7). Although those studies have encompassed a wide range of Mach numbers, they have been restricted to the high Reynolds number range which does not indicate the viscous interaction effects which planetary entry vehicles encounter at very high altitudes.

For the speed regime of satellite vehicles entering the Earth's atmosphere, the necessity of minimizing convective heating led to blunt shapes for payload housing. However, as velocities increase to interplanetary speeds radiation heating assumes a more important role than does convective heating, reviving interest in the more slender configurations. When the roles of drag coefficient and heat-transfer coefficient are considered in minimizing the ratio of heat transfer to drag coefficients (Ref. 8), the desired body fineness ratio then is much smaller. Because earlier experiments have revealed the effect of low Reynolds numbers on the drag of a type of blunt body of interest for planetary probes and Earth satellites (Ref. 9), it was believed worthwhile to investigate the drag of the same shape after modification to what might be considered a low-drag, low-radiation-heating configuration by addition of a nose spike. While the effect of a spike is well known in general, it was doubted if the effect would be as favorable under simulated high-altitude conditions.

In order to extend available data into the rarefied flow regime, an investigation was conducted in the low-density, hypersonic tunnel (Gas Dynamic Wind Tunnel, Hypersonic (L)) of the von Kármán Gas Dynamics Facility (VKF), at the Arnold Engineering Development Center (AEDC), Air Force Systems Command (AFSC). This report contains results of this investigation concerning the aerodynamic drag at various angles of attack for a Mach number of 10.1 and Reynolds number, based on model wetted length, from 200 to 1200.

2.0 APPARATUS

2.1 WIND TUNNEL

Tunnel L is a continuous, arc-heated, ejector-pumped, low-density wind tunnel. The major components are (1) a d-c arc heater of the

Manuscript received July 1964.

constricted-arc type with a 40-kv power supply, (2) a settling section
of variable length but normally about 6 in. long, (3) a contoured aero-
dynamic nozzle with uniform test section fluid properties, (4) a test
chamber of 48-in. diameter surrounding the test section and contain-
ing instrumentation and probe carrier, (5) an interchangeable diffuser,
(6) a heat exchanger, (7) an air ejector of two stages, and (8) the VKF
vacuum pumping system. All critical components of the tunnel are
protected by back-side water cooling. The two-stage ejector system
is driven by air instead of steam because of the ready availability of
the former in the present case. The working gas in this case was
nitrogen. A more detailed description of the tunnel is given in Ref. 10.

2.2 DRAG BALANCE

Although of small size, Tunnel L is suitable for aerodynamic-force
tests if small models are used and a balance capable of measuring the
extremely small aerodynamic loads is available. The one-component
balance utilized throughout these tests is capable of good accuracy even
when full-scale loads as low as 0.02 lb are of concern. Figure 1 shows
the balance with a model in Tunnel L.

The balance has an internal parallelogram-type structure, with the
deflection being proportional to the force applied along the axis of the
sting. The deflection is sensed with a linear variable differential trans-
former with a 0.005-in. linear range. Approximately 0.003-in. deflec-
tion of the balance is equivalent to 0.3 lb.

Calibration of the balance* was performed several times during
the period of tunnel operation. Figure 2 shows typical calibrations,
indicating the repeatability of the calibration constant. Aerodynamic
drag loads were on the order of 0.01 lb during the test. The effect of
normal-force interaction was studied by placing dummy loads on the
balance sting greater than the expected normal-force loads during the
test, and the interaction was found to be negligible. Because the balance
only measures forces parallel to the sting, to measure drag at angles of
attack, models must be constructed with appropriate provisions to
achieve a range of angles of attack. In the present case, this was accom-
plished by fabricating separate models.

_____

*This balance was developed by the Transducer Development
Section, Instrumentation Branch, VKF, under the supervision of
D. S. Bynum.

2.3 MODELS

The basic configuration of the models is a 10-deg semi-vertex blunted cone with a modified spherical nose segment and a right circular cylinder. The right circular cylinder was tested with its axis of symmetry parallel to the flow centerline. The models are shown in Figs. 3 and 4, with the basic dimensions indicated in Fig. 4. For purposes of data reduction, the characteristic length is defined as: (1) the length measured along the surface of the model from the stagnation point of the hemispherical nose to the rim of the flat base, plus the axial length of the spike, for the Mars entry body, and (2) the total axial length from the spike tip to the flat base for the right circular cylinder. After fabrication, the models were inspected with an optical comparator, and the angles of attack were measured as given in Fig. 4.

3.0 EXPERIMENTAL PROCEDURE

The test models were placed on the balance sting at a predetermined station in the test region of the nozzle. The models were first tested at a positive angle of attack, then rotated 180 deg and tested at a negative angle of attack. Run duration was limited to not more than approximately 20 sec to prevent excessive heating of the balance components and to retain the relatively cold-wall model conditions.

The right circular cylinder was tested only at 0-deg angle of attack.

Shown in Fig. 5 are impact-pressure profiles for the stations in the nozzle where the models were placed for testing. The nozzle used is a Mach 10, completely contoured, 0.1481-in.-diam-throat nozzle. The surveys show that the nozzle is completely free of axial gradients in the test section. Test conditions were p_O = 18 psia, T_O = 5625°R, M_∞ = 10.1, and Re_∞/in. = 388.

4.0 RESULTS AND DISCUSSION

The models were tested at both positive and negative angles of attack to check for flow angularity in the free-stream. Since no angularity was obviously present, all data have been plotted without distinction, except in the case of Fig. 6. During these runs the sting mount was found to be at a negative 2-to-3-deg angle of attack, thereby requiring the zero-shift found in Fig. 6.

The data have been reduced to coefficient form and are presented as functions of both L_{spike}/D_{base} and the viscous interaction parameter (cf. Ref. 11),

$$\bar{V}_\infty = M_\infty \sqrt{C_\infty \cdot Re_{\infty,L}}$$

where

$$C_\infty = (\mu_w T_\infty) / (\mu_\infty T_w)$$

and

$$Re_{\infty,L} = U_\infty \rho_\infty L / \mu_\infty$$

and L is the body length as defined in Fig. 4 and Section 2.3. The coefficient $(C_\infty)^{1/2}$ was essentially constant (≈ 0.83) for this investigation.

A comparison of all data at each angle of attack is shown in Fig. 6. Some data show variations of ± 10 percent, although in the majority of the cases the maximum scatter is on the order of ± 5 percent.

In order to retain the relatively cold-wall conditions desired, the models were allowed to remain in the flow on the average of only 10 to 20 sec. It has been shown (cf. Refs. 11 and 12) that the aerodynamic drag in low-density, hypersonic flow is a function of the wall-to-stagnation temperature ratio, T_w/T_0. The scatter indicated in Fig. 6 could be caused by slight variations in model wall temperature, although there is no systematic variation indicated by the data. The value of T_w/T_0 was estimated for the present tests to be 0.2.

Figure 7 indicates that as $\bar{V}_\infty \longrightarrow 0$ the viscous effects are reduced, as found in earlier studies. Here it may be noted that the reduction in $\bar{V}_\infty$ for the present tests was obtained by increasing the model characteristic length, L, whereas in Ref. 9 the variation was obtained by changing the flow conditions. The correlation of the spiked body data with the basic body of Ref. 9 is very good considering the differences in the fore-bodies.

As is noted in earlier studies, for bluff bodies such as the right circular cylinder, drag coefficients may be reduced by more than an order of magnitude (cf. Ref. 1) in high Reynolds number cases using the sharp spikes. However, as shown in Figs. 7 and 8, no such marked reduction occurs for the density altitude simulated here. Although a reduction of 27 percent in drag is realized, the length of spike required to accomplish this (5.0 D_{base}) may be prohibitively long.

The variation of C_D with $\bar{V}_\infty$ is shown in Fig. 9. Here a very revealing effect occurs which is undoubtedly due to the predominant viscous

effects on the spikes. Whereas in earlier studies reductions in C_D were realized even at large angles of attack when spikes were incorporated in the body, this is no longer true for the present tests: for increasing spike length and angle of attack above approximately 25 deg, the spike has the effect of increasing the drag.

The value of about 25 deg for maximum angle of attack at which a drag reduction may be expected for various spike lengths is clearly demonstrated in Fig. 10. Here it may be seen that the drag coefficient is essentially constant for a variable spike length at an approximate value of angle of attack of 24 deg.

Following the analysis of Ref. 9, Fig. 11 is prepared showing the correlation of the normalized parameter, C_D^*, with the viscous interaction parameter, $\bar{V}_\infty$. Included in Fig. 11, from Ref. 9, are data obtained at 0-deg angle of attack, which have been correlated with the present tests for varying spike lengths ($0 \leq L_{spike}/D_{base} \leq 5$). The degree of correlation is indeed gratifying, showing the removal of forebody shape dependence. The effects were removed by normalizing the data using the parameter of Ref. 9,

$$C_D^* = (C_D - C_{D_i})(C_{D_{FM}} - C_{D_i})$$

When C_D^* is plotted as a function of the viscous interaction drag parameter, $\bar{V}_\infty$, for sufficiently rarefied flow, C_D^* will approach 1.0, and for nearly inviscid flow, C_D^* will approach 0.0.

The correlation of the spiked body drag with that of Ref. 9 is seen to be much better in Fig. 11 as compared to that given in Fig. 7. The values of C_{D_i} used in Fig. 11 were obtained from Ref. 14.

Data corresponding to minimum and maximum values of $\bar{V}_\infty$ for the range of angle of attack from 0 to 40 deg have been plotted in Fig. 12, which compares the data to both modified Newtonian theory and the theory for free-molecule flow (Ref. 13). Simulation well into the transition regime between continuum, inviscid-fluid flow, and free-molecule flow was achieved. It was assumed that the incident molecules were at T_∞, the reflected molecules at T_W, and the wall temperature was constant over the model.

5.0 CONCLUDING REMARKS

Aerodynamic drag has been determined for a short 10-deg blunted cone and a right circular cylinder with spikes as forebodies in a flow

5

regime in which viscous interaction effects are significant. Comparison of the data to inviscid, modified Newtonian, and free-molecule theory indicates that the drag coefficient was affected significantly by viscous-fluid effects.

Reductions in drag coefficient for small angles of attack and $0 \leq L_{spike}/D_{base} \leq$ were realized, although, contrary to high Reynolds number cases, increase in drag were obtained for the large angles of attack (≥ 25 deg) with spike length increasing. Approximately 25-percent reductions in C_D were obtained at 0-deg angle of attack. However, this magnitude of reduction in drag is far less than has been found to occur at high Reynolds numbers.

Correlation of the data for spiked and unspiked bodies by using the parameter C_D^* (suggested by J. L. Potter for use in Ref. 9) indicates that the model shape dependence of C_D was largely removed. This suggests a method for estimating approximate drag coefficients of a wide variety of similar shapes by obtaining inviscid and free-molecular drag coefficients and referring to the correlation curve presented herein.

REFERENCES

1. Bogdonoff, S. M., and Vas, I. E. "Preliminary Investigations of Spiked Bodies at Hypersonic Speeds." Princeton University, WADC-TN-58-7 (AD 142280), March 1958.

2. Hunt, G. K. "Supersonic Wind-Tunnel Study of Reducing the Drag of a Bluff Body at Incidence by Means of a Spike." Royal Aircraft Establishment, Report No.: AERO. 2606, May 1958.

3. Moeckel, W. E. "Flow Separation Ahead of a Blunt Axially Symmetric Body at Mach Numbers 1.76 to 2.10." NACA RM E51I25, December 1951.

4. Jones, Jim J. "Experimental Drag Coefficients of Round Noses with Conical Windshields at Mach Number 2.72." NACA RM L55E10, June 1955.

5. Jones, Jim J. "Flow Separation from Rods Ahead of Blunt Noses at Mach Number 2.72." NACA RM L52E05a, July 1962.

6. Beastall, D. and Turner, J. "The Effect of a Spike Protruding in Front of a Bluff Body at Supersonic Speeds." Aeronautical Research Council, R. & M. No. 3007, January 1952.

7. Album, Hyman H. "Spiked Blunt Bodies in Supersonic Flow." AFOSR Rept. 307, June 1961.

8. Allen, H. Julian. "Hypersonic Aerodynamic Problems of the Future." Presented to the Fluid Mechanics Panel of Advisory Group for Aeronautical Research and Development, Brussels, Belgium, April 3-6, 1962.

9. Boylan, David E. and Sims, William H. "Experimental Determination of Aerodynamic Drag on a Blunted 10-deg Cone at Angles of Attack in Hypersonic, Rarefied Flow." AEDC-TDR-64-SO (AD 435860), April 1964.

10. Potter, J. L. "Low-Density, Hypersonic (LDH) Wind Tunnel L." von Kármán Gas Dynamics Facility, ARO, Inc., Technical Developments (Ed. by J. Lukasiewicz, 1964) pp. 61-63.

11. Lukasiewicz, J., Whitfield, Jack D., and Jackson, R. "Aerodynamic Testing at Mach Numbers from 15 to 20." Hypersonic Flow Research, Edited by Frederick R. Riddell, Academic Press, New York, 1962.

12. Kinslow, M. and Potter, J. L. "Drag of Spheres in Rarefied Hypervelocity Flow." AIAA Journal, Vol. I, No. 11, November 1963, pp. 2467-2473.

13. Sentman, Lee H. "Free Molecule Flow Theory and Its Application to the Determination of Aerodynamic Forces." Lockheed Missile and Space Co., LMSC-448514, October 1961.

14. Clark, E. L. and Trimmer, L. L. "Equations and Charts for the Evaluation of the Hypersonic Aerodynamic Characteristics of Lifting Configurations by the Newtonian Theory." AEDC-TDR-64-25 (AD 431848), March 1964.

Fig. 1 Balance and Model Mounted in Tunnel L
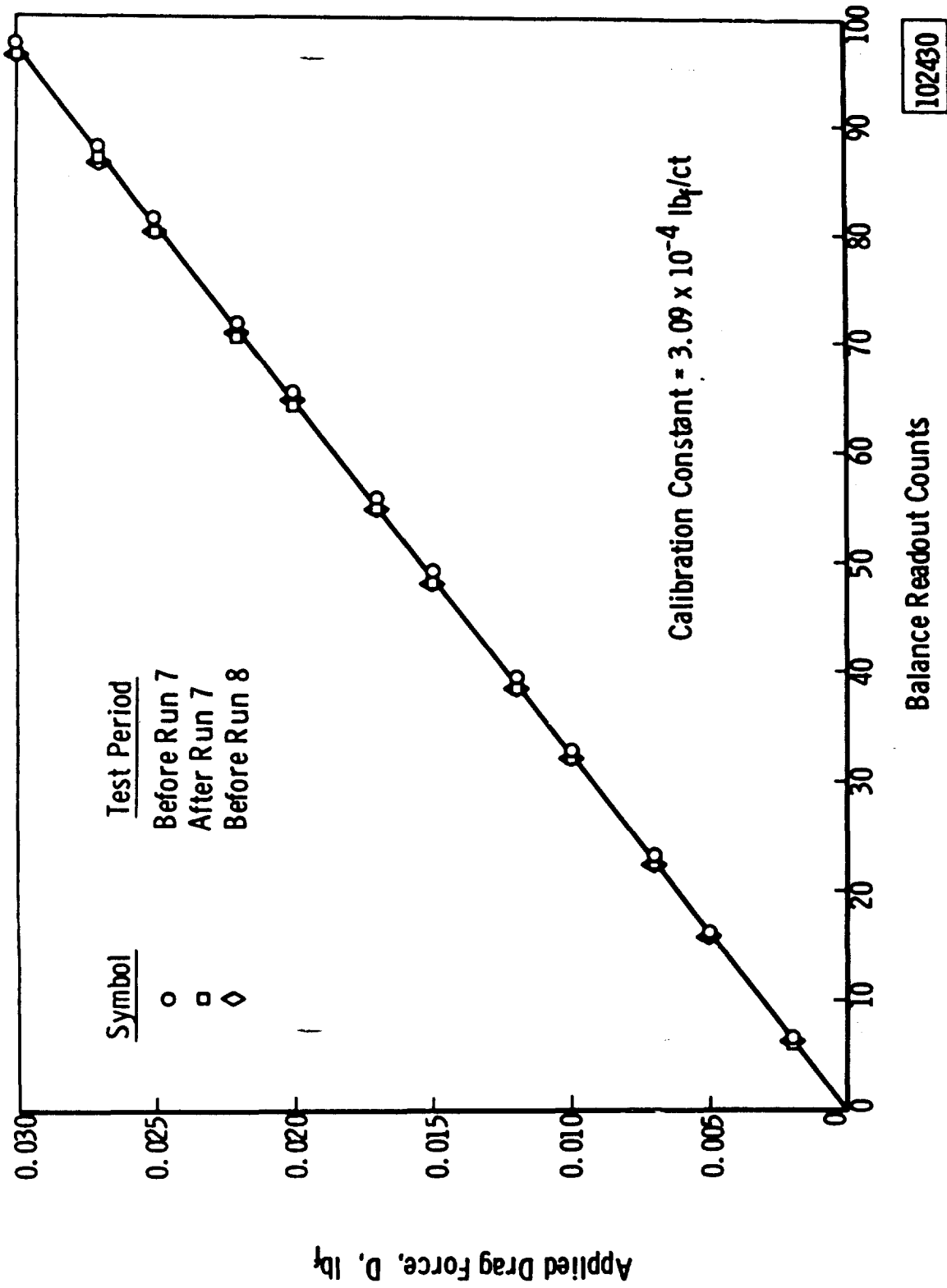
Fig. 2 Typical Balance Calibration

AEDC
46359-U
102431

Fig. 3 Photograph of Models

11
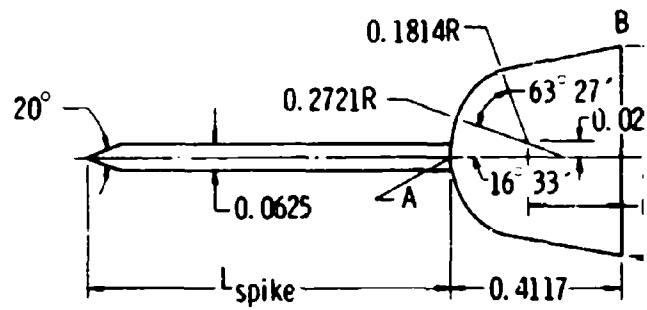
All Dimensions in Inches
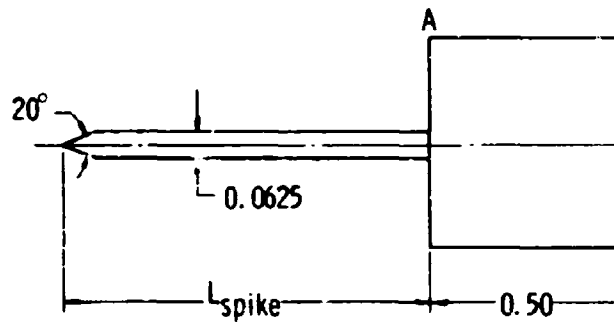
Fig. 4

00
266

∠
⊏10°
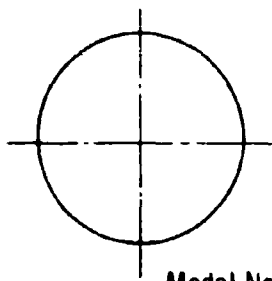
Model No.	Angle of Attack
1	0
2	$10°$
3	$20°$
4	$31° 26'$
5	$40°$

Mars Probe
$L = 0.542 + L_{spike}$ °

0.50
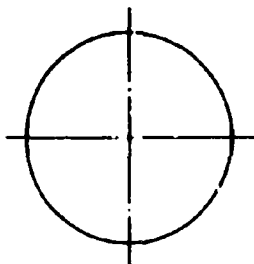
Right Circular Cylinder
$a = 0°$, $L = 0.50 + L_{spike}$ °

°The length L is defined as the
distance AB in the sketch plus L_{spike}.

102432

Model Dimensions
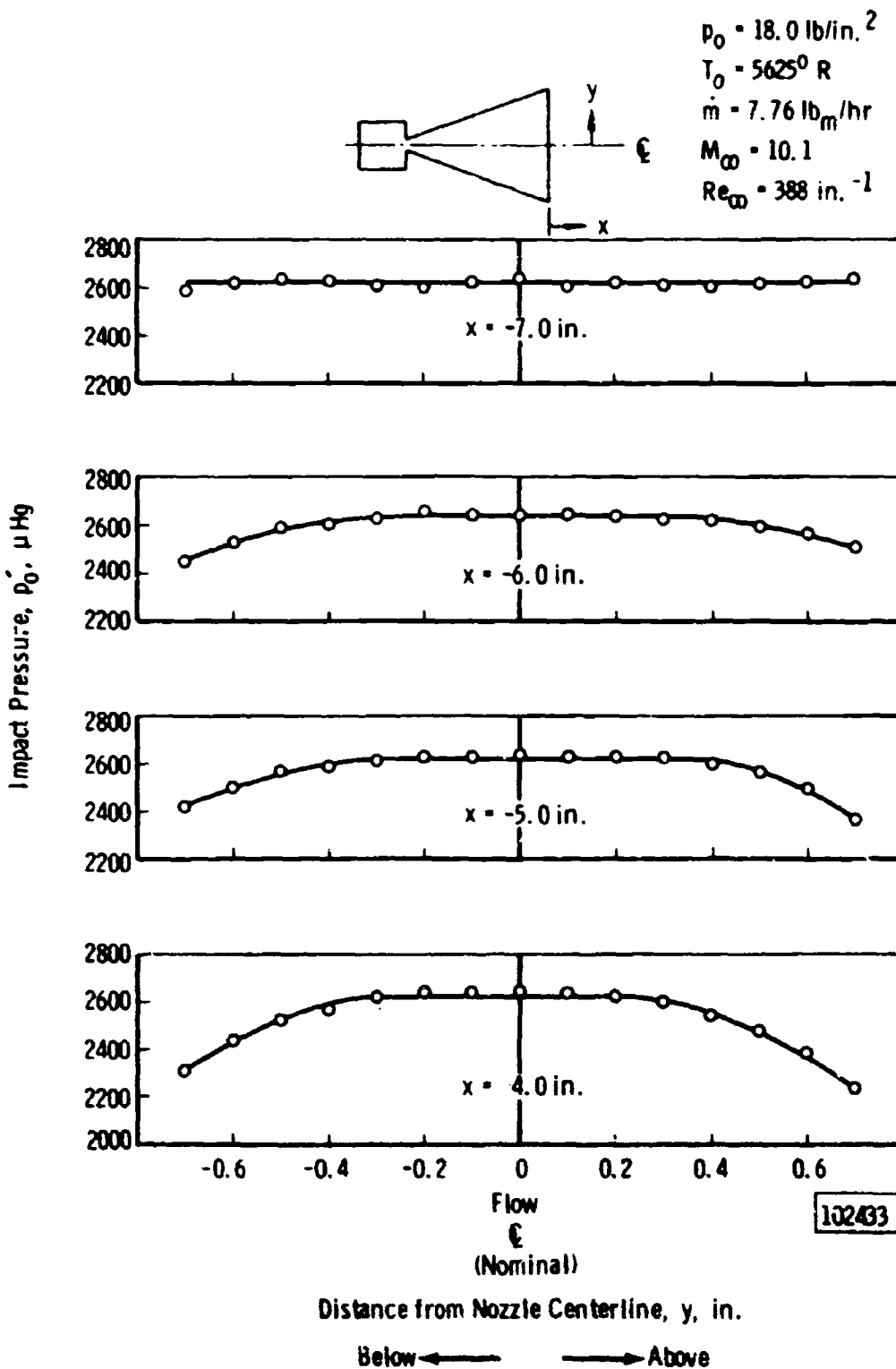
Fig. 5 Radial Impact Pressure Surveys of Nozzle
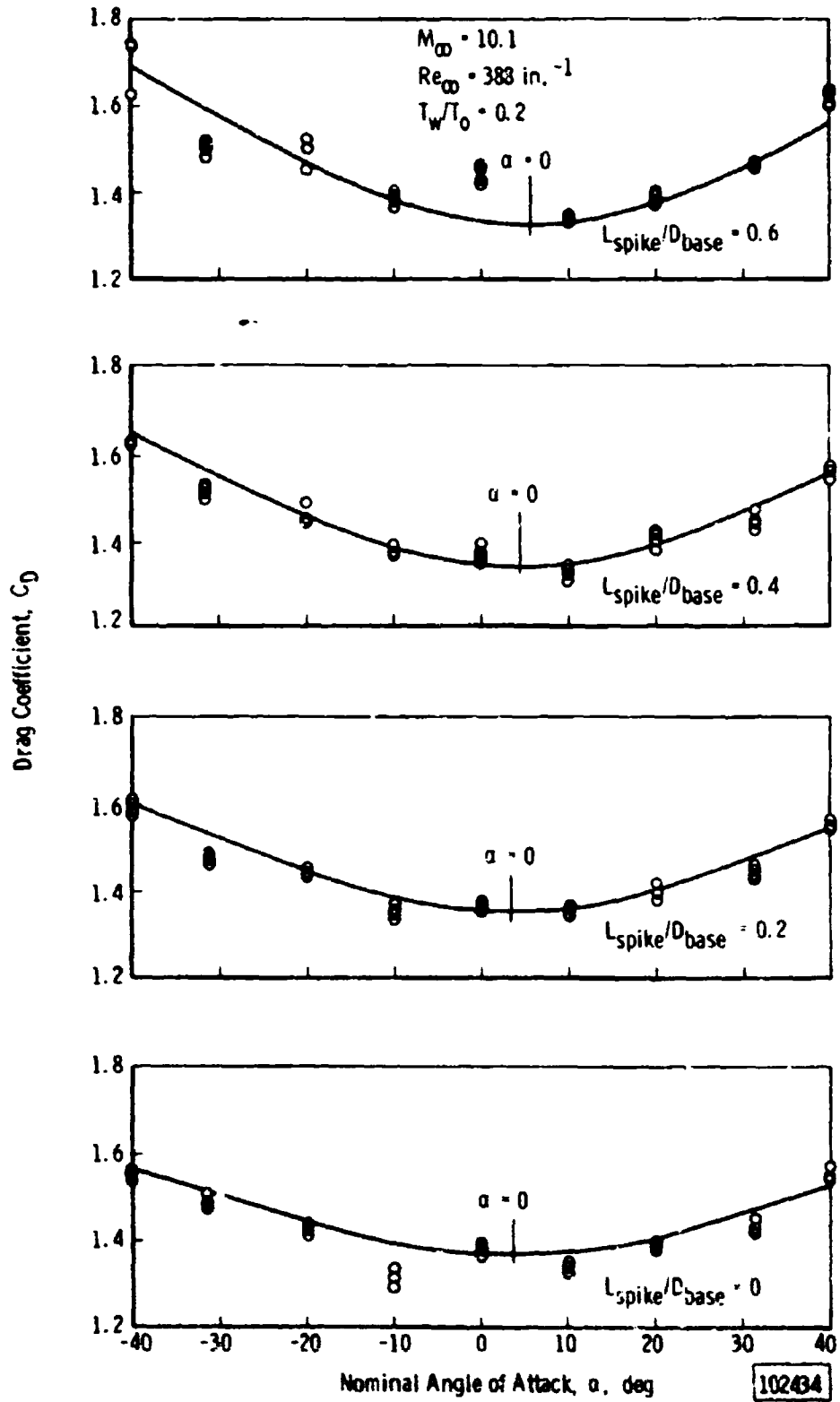
Fig. 6 Drag Coefficient as a Function of Angle of Attack

Fig. 6 Concluded

Symbol	T_W/T_0	γ	M_∞	
●	0.20	1.4	10.1	Present
▲	0.20	1.4	10.1	Tests
◨	0.30	1.67	8.12-12.32	
△	0.20	1.67	7.49-8.73	Ref. 9
◇	0.25	1.4	9.60-10.10	
◻	0.25	1.4	10.17	

Spiked Right Cylinder

Note: Variation of $\bar{v}_\infty$ in Present Tests Obtained by Varying L_{spike} with $Re_\infty = 388$ in.$^{-1}$

Variation of $\bar{v}_\infty$ in Ref. 9 Obtained by Varying Flow Conditions.

Mars Probe

$\alpha = 0^\circ$

$$\bar{v}_\infty = M_\infty \sqrt{C_\infty/Re_{\infty, L}}$$

4.2 2.6   1.2   0.4
5.0 3.4 1.8   0.8   0
4.6 3.0   1.38   0.6
3.8 2.2   1.0   0.2

102436

L_{spike}/D_{base}
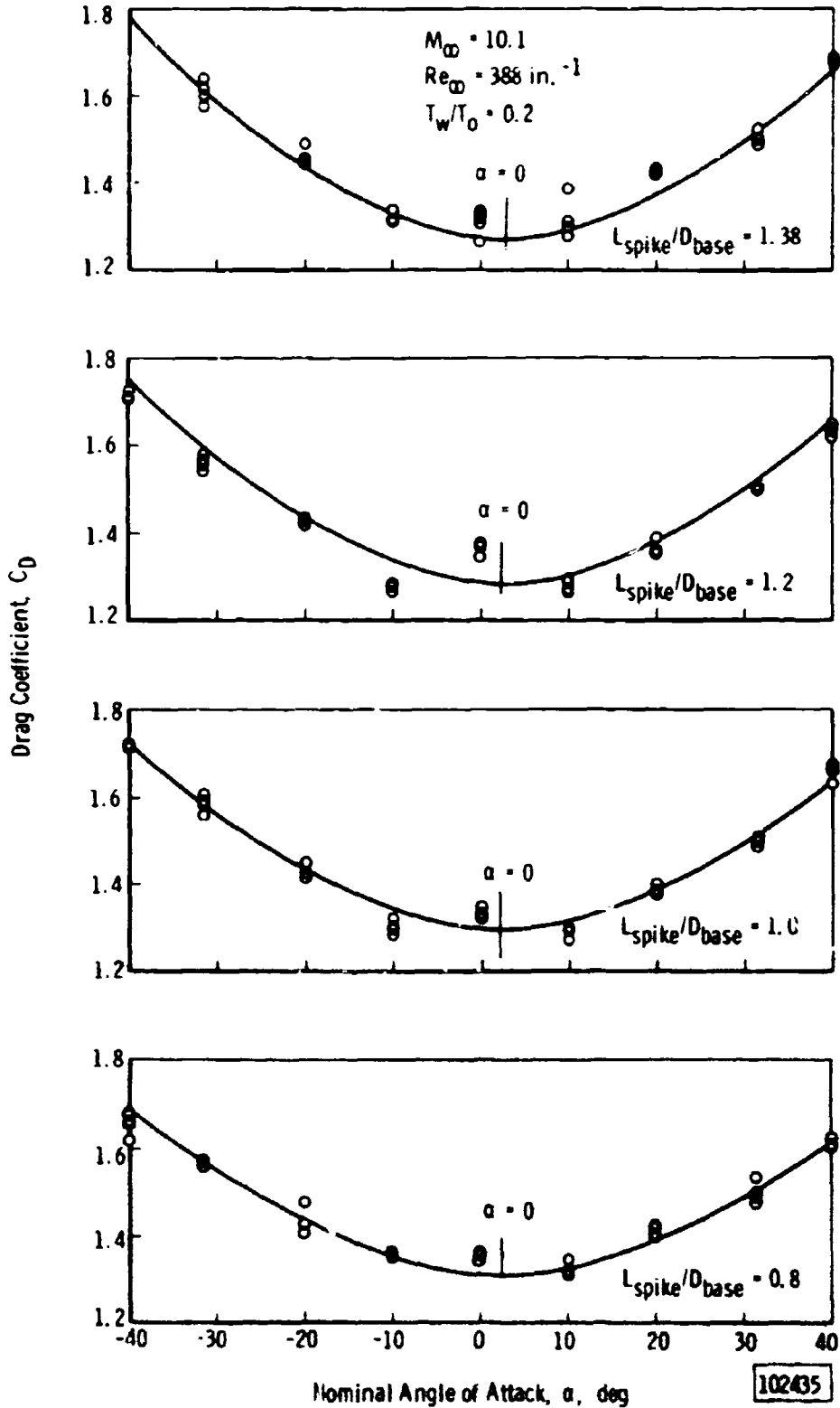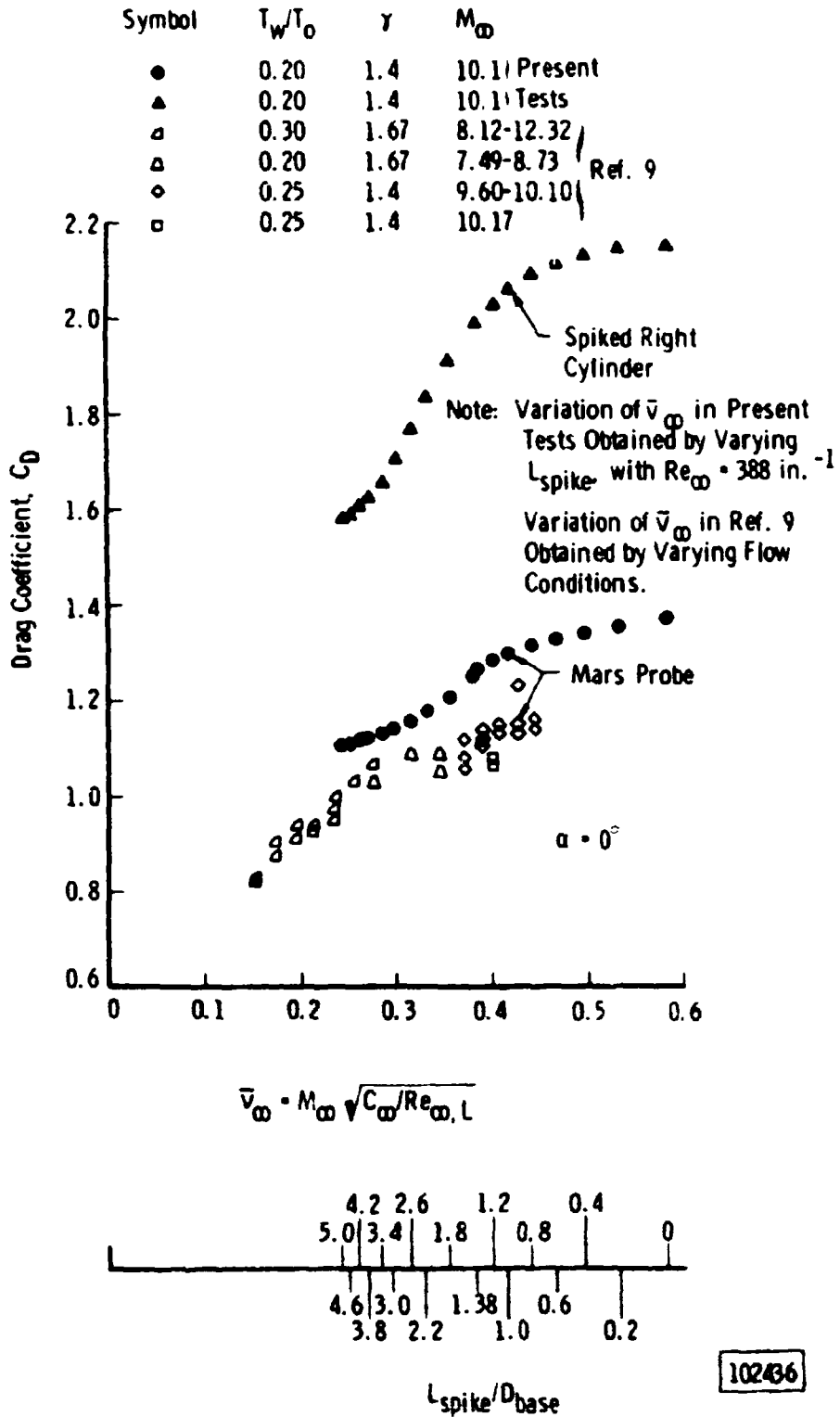
Fig. 7 Drag Coefficient as a Function of $\bar{v}_\infty$ ($\alpha = 0$ deg)

16
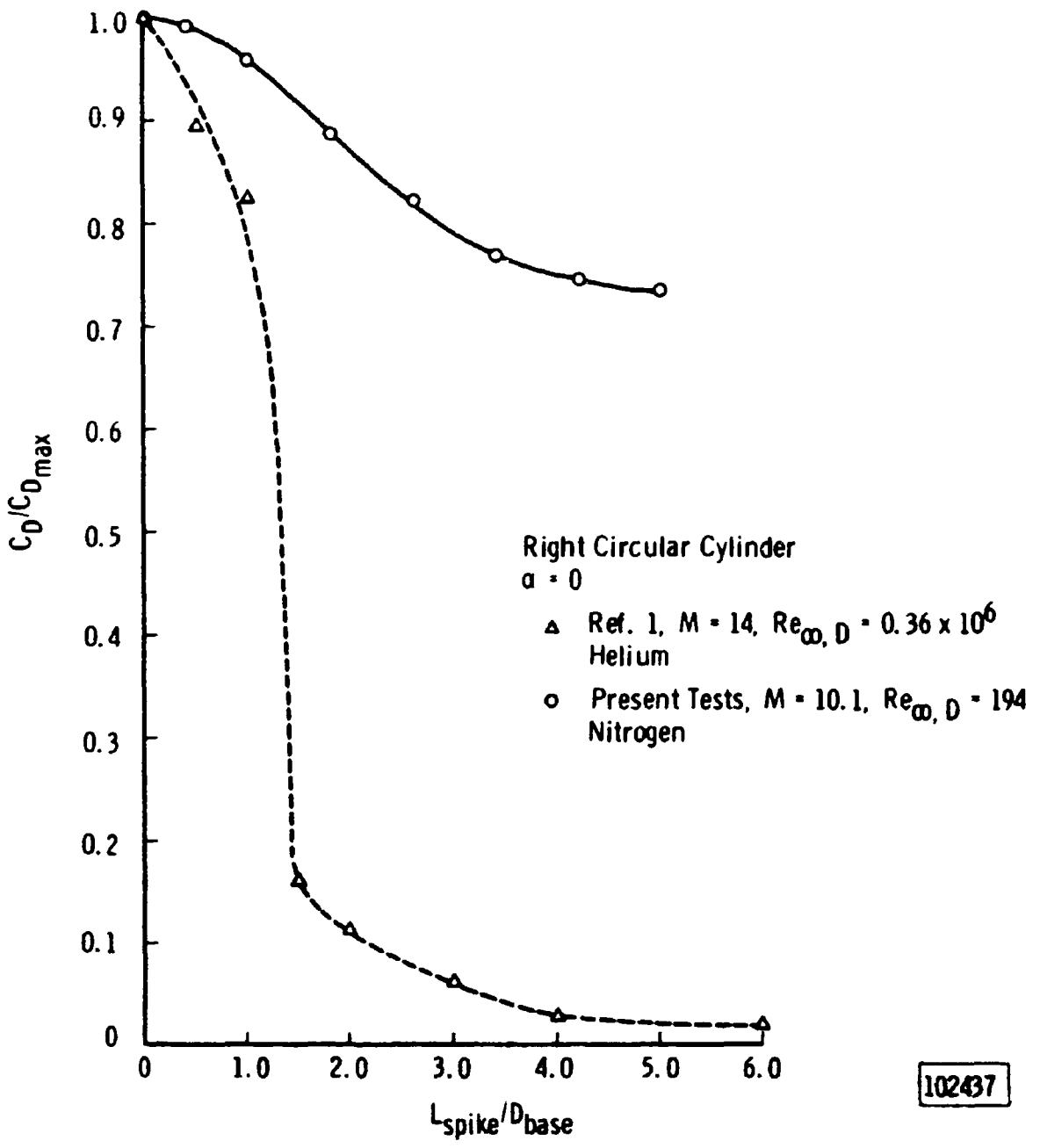
Fig. 8 Drag Coefficient Ratio, $C_D / C_{D_{max}}$, as a Function of Spike Length for the Right Cylinder
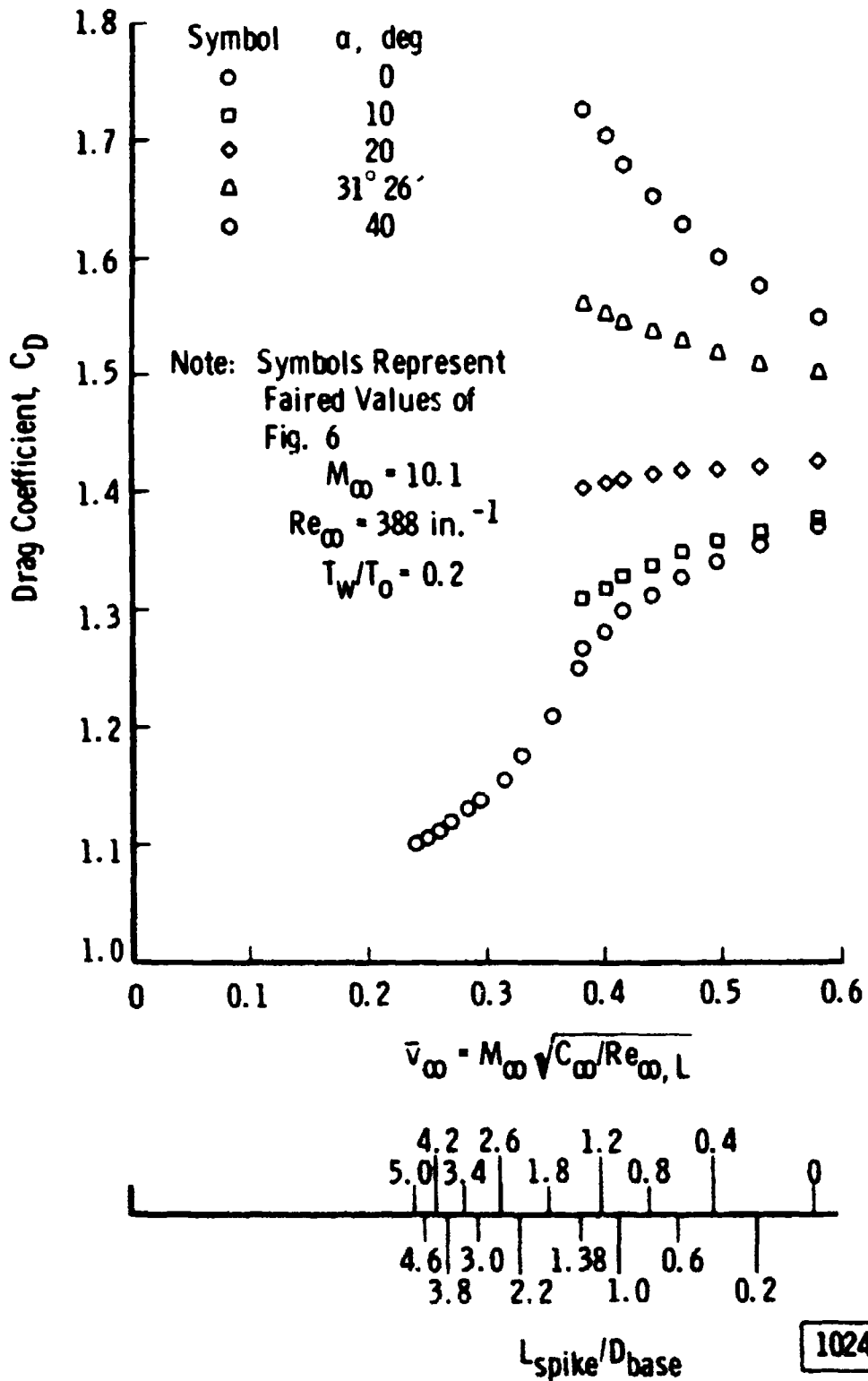
Fig. 9 Drag Coefficient of Mars Probe as a Function of $\bar{v}_\infty$ for Varying Angle of Attack
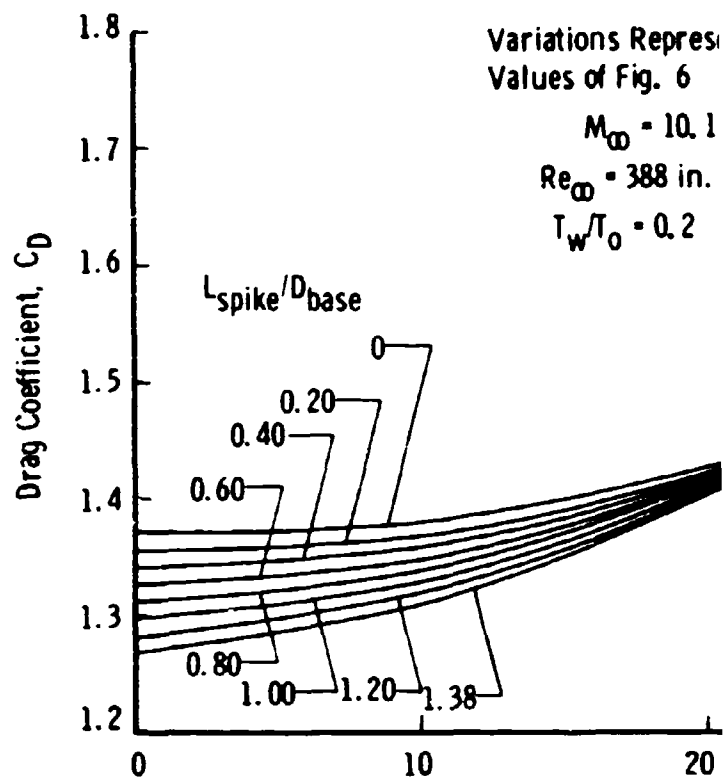
Fig. 10 Drag Coefficient of the Mars Probe a

The figure shows Drag Coefficient, C_D (y-axis, ranging 1.2 to 1.8) plotted against an x-axis (0 to 20). Annotations include:

Variations Repres
Values of Fig. 6

$M_\infty = 10.1$
$Re_\infty = 388$ in.
$T_w/T_0 = 0.2$

L_{spike}/D_{base} curves labeled: 0, 0.20, 0.40, 0.60, 0.80, 1.00, 1.20, 1.38

Faired

L_{spike}/D_{base}

1.38
1.20
1.00
0.80
0.60
0.40
0.20
0

30   40   50
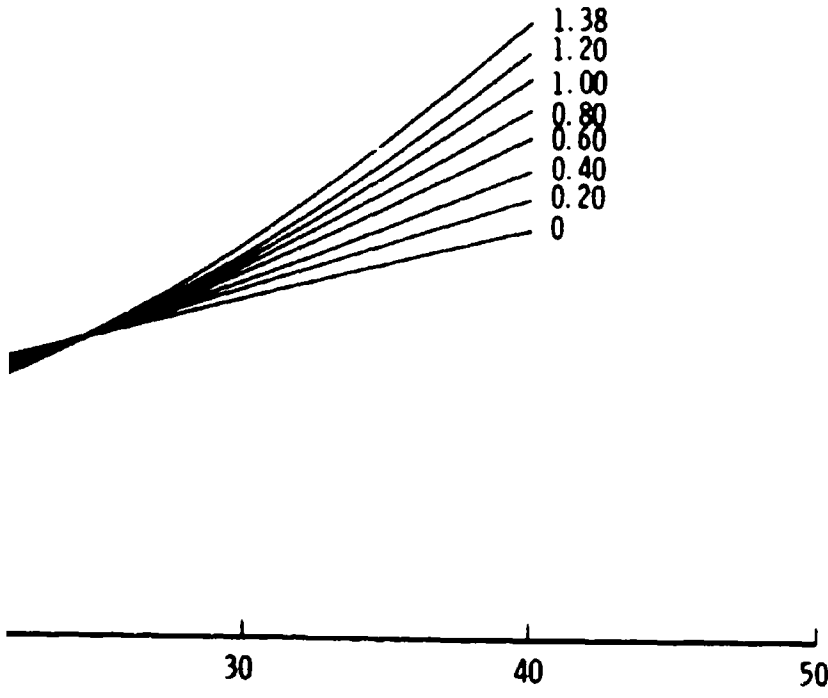
gle of Attack, α, deg   102439

Function of Angle of Attack for Varying L_{spike}/D_{base}

AEDC-TDR-64-160

Symbol	M_∞	α, deg	Model	T_w/T_0	γ	Tests
$\circ$	10.1	0	Mars	0.20	1.4	Present
$\blacktriangle$	7.49-12.32	0	Mars	0.20-0.30	1.4 & 1.67	Ref. 9

Variation of $\bar{v}_\infty$ in Present Tests Obtained by Varying the Spike Length with $Re_\infty = 388$ in.$^{-1}$. Data Points Are Faired Values from Fig. 6.

Variation of $\bar{v}_\infty$ in Ref. 9 Obtained by Varying the Flow Conditions.
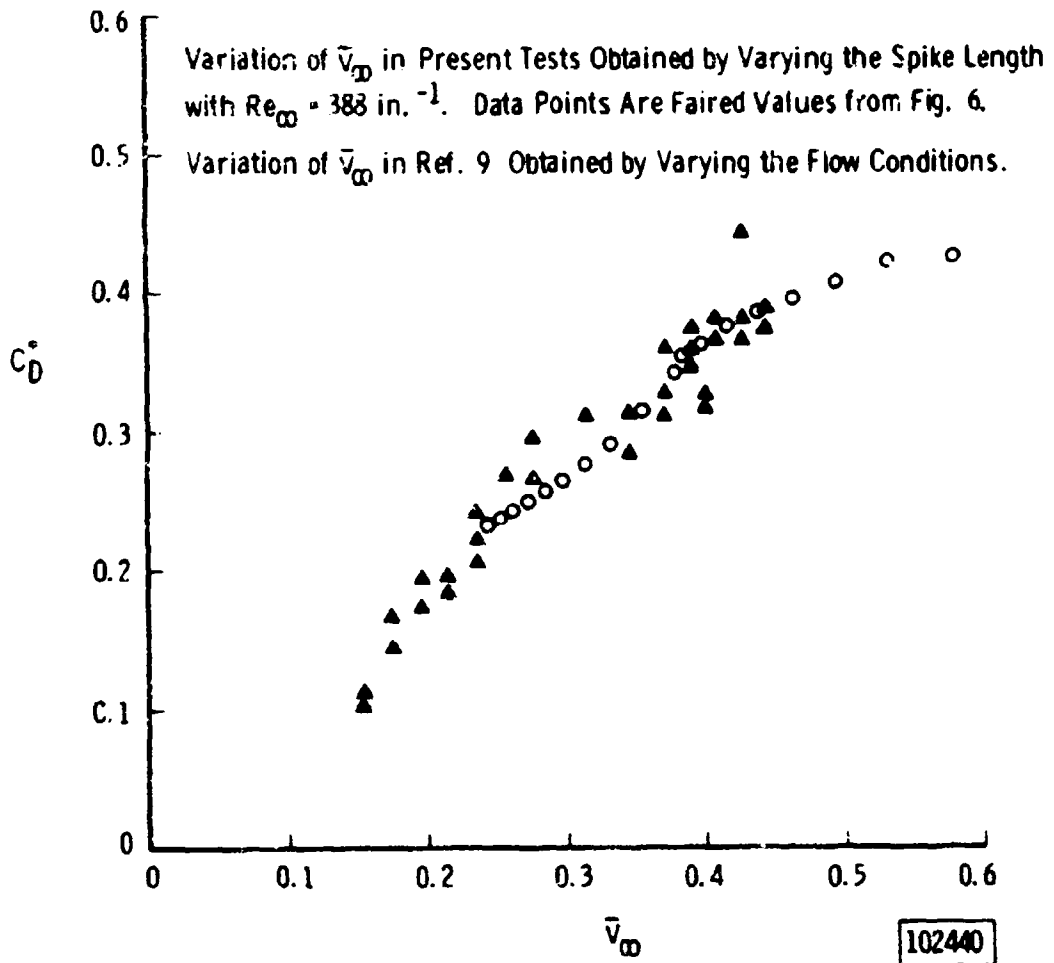
102440

Fig. 11 Normalized Drag Coefficient, C_D^*, as a Function of $\bar{v}_\infty$ for the Mars Probe

Symbol	Model	$\bar{V}_\infty$
○	Mars Probe	0.578
△	Mars Probe	0.383

Data Points Represent
Faired Values from Fig. 6.

Drag Coefficient, C_D
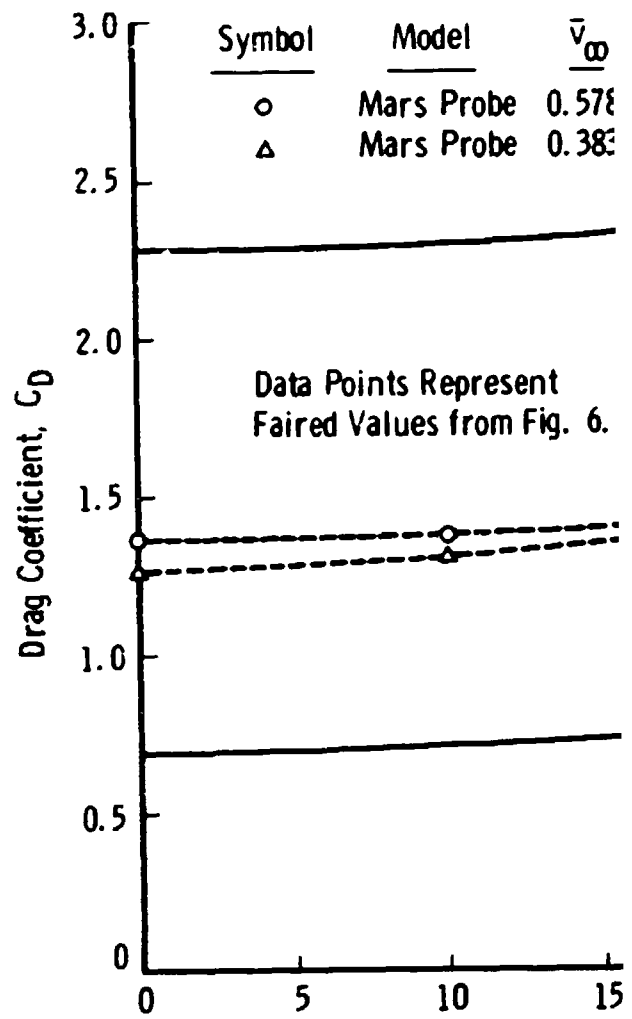
Fig. 12 Drag Coefficient as a Func

L_{spike}/D_{base}	M_∞	Re_∞
0	10.1	388 in.$^{-1}$
1.38	10.1	388 in.$^{-1}$

$$\left\{\begin{array}{l} \text{Free Molecule} \\ S = 8, \ T_w/T_0 = 4.32 \\ L_{spike} = 0, \ \text{Ref. 13} \end{array}\right\}$$

$$\left\{\begin{array}{l} \text{Modified Newtonian} \\ \gamma = 1.4, \ L_{spike} = 0 \\ \text{Ref. 14} \end{array}\right\}$$
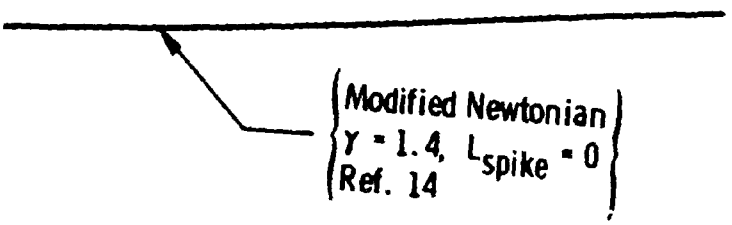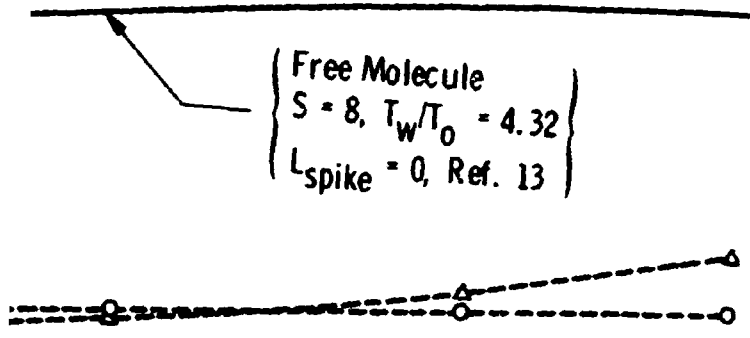
Angle of Attack, α, deg

20 25 30 35 40

102441

n of Angle of Attack at Constant Values of $\tilde{v}_\infty$